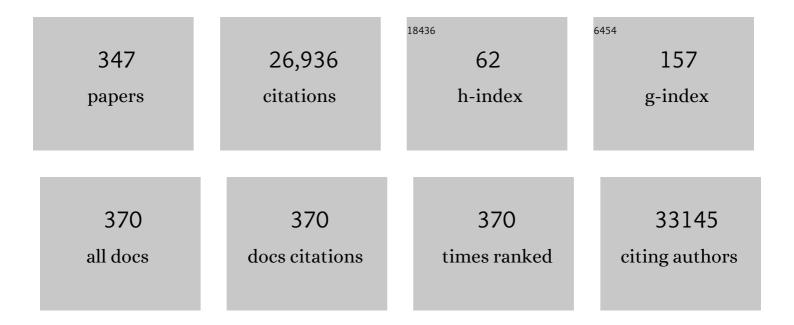
Gianluigi A Botton

List of Publications by Year in descending order

Source: https://exaly.com/author-pdf/6580756/publications.pdf Version: 2024-02-01



#	Article	IF	CITATIONS
1	Electron-energy-loss spectra and the structural stability of nickel oxide:â€,â€,An LSDA+U study. Physical Review B, 1998, 57, 1505-1509.	1.1	10,657
2	Platinum single-atom and cluster catalysis of the hydrogen evolution reaction. Nature Communications, 2016, 7, 13638.	5.8	1,521
3	Single-atom Catalysis Using Pt/Graphene Achieved through Atomic Layer Deposition. Scientific Reports, 2013, 3, .	1.6	719
4	Size-Selected Synthesis of PtRu Nano-Catalysts:  Reaction and Size Control Mechanism. Journal of the American Chemical Society, 2004, 126, 8028-8037.	6.6	672
5	Polymerization from the Surface of Single-Walled Carbon Nanotubes â^' Preparation and Characterization of Nanocomposites. Journal of the American Chemical Society, 2003, 125, 16015-16024.	6.6	462
6	Nanocrystalline intermetallics on mesoporous carbon for direct formic acid fuel cell anodes. Nature Chemistry, 2010, 2, 286-293.	6.6	448
7	Atomic layer deposited Pt-Ru dual-metal dimers and identifying their active sites for hydrogen evolution reaction. Nature Communications, 2019, 10, 4936.	5.8	371
8	Comparison of Single Crystal and Polycrystalline LiNi _{0.5} Mn _{0.3} Co _{0.2} O ₂ Positive Electrode Materials for High Voltage Li-Ion Cells. Journal of the Electrochemical Society, 2017, 164, A1534-A1544.	1.3	280
9	p-Type Modulation Doped InGaN/GaN Dot-in-a-Wire White-Light-Emitting Diodes Monolithically Grown on Si(111). Nano Letters, 2011, 11, 1919-1924.	4.5	255
10	Multipolar Plasmonic Resonances in Silver Nanowire Antennas Imaged with a Subnanometer Electron Probe. Nano Letters, 2011, 11, 1499-1504.	4.5	240
11	Electronic Structure and Elastic Properties of Strongly Correlated Metal Oxides from First Principles: LSDA + U, SIC-LSDA and EELS Study of UO2 and NiO. Physica Status Solidi A, 1998, 166, 429-443.	1.7	203
12	Controlling Electron Overflow in Phosphor-Free InGaN/GaN Nanowire White Light-Emitting Diodes. Nano Letters, 2012, 12, 1317-1323.	4.5	178
13	A Model for the Ultrastructure of Bone Based on Electron Microscopy of Ion-Milled Sections. PLoS ONE, 2012, 7, e29258.	1.1	171
14	The role of vacancies and defects in Na0.44MnO2 nanowire catalysts for lithium–oxygen batteries. Energy and Environmental Science, 2012, 5, 9558.	15.6	169
15	The Impact of Electrolyte Additives and Upper Cut-off Voltage on the Formation of a Rocksalt Surface Layer in LiNi _{0.8} Mn _{0.1} Co _{0.1} O ₂ Electrodes. Journal of the Electrochemical Society, 2017, 164, A655-A665.	1.3	161
16	Copper adparticle enabled selective electrosynthesis of n-propanol. Nature Communications, 2018, 9, 4614.	5.8	153
17	Full-Color Single Nanowire Pixels for Projection Displays. Nano Letters, 2016, 16, 4608-4615.	4.5	151

18 Mixed-quantum-dot solar cells. Nature Communications, 2017, 8, 1325.

5.8 148

#	Article	IF	CITATIONS
19	Materials science applications of HREELS in near edge structure analysis and low-energy loss spectroscopy. Ultramicroscopy, 2003, 96, 535-546.	0.8	145
20	Controlled orientation of liquid-crystalline polythiophene semiconductors for high-performance organic thin-film transistors. Applied Physics Letters, 2005, 86, 142102.	1.5	130
21	Plasmonic Response of Bent Silver Nanowires for Nanophotonic Subwavelength Waveguiding. Physical Review Letters, 2013, 110, 066801.	2.9	127
22	Enhanced and tunable surface plasmons in two-dimensional <mml:math xmlns:mml="http://www.w3.org/1998/Math/MathML"><mml:mrow><mml:msub><mml:mi>Ti</mml:mi><mml:mn mathvariant="normal">C<mml:mn>2</mml:mn></mml:mn </mml:msub></mml:mrow>stacks: Electronic structure versus boundary effects. Physical Review B, 2014, 89, .</mml:math 	>3 _{ /mml: 1.1	mn>122
23	Elucidating the Nature of the Active Phase in Copper/Ceria Catalysts for CO Oxidation. ACS Catalysis, 2016, 6, 1675-1679.	5.5	122
24	Chemical Structure of Nitrogen-Doped Graphene with Single Platinum Atoms and Atomic Clusters as a Platform for the PEMFC Electrode. Journal of Physical Chemistry C, 2014, 118, 3890-3900.	1.5	121
25	Soluble, Discrete Supramolecular Complexes of Single-Walled Carbon Nanotubes with Fluorene-Based Conjugated Polymers. Macromolecules, 2008, 41, 2304-2308.	2.2	120
26	Nanoscale Manipulation of Spinel Lithium Nickel Manganese Oxide Surface by Multisite Ti Occupation as Highâ€Performance Cathode. Advanced Materials, 2017, 29, 1703764.	11.1	119
27	Synthesis of Single Crystal LiNi _{0.88} Co _{0.09} Al _{0.03} O ₂ Âwith a Two-Step Lithiation Method. Journal of the Electrochemical Society, 2019, 166, A1956-A1963.	1.3	117
28	Encapsulation of Conjugated Oligomers in Singleâ€Walled Carbon Nanotubes: Towards Nanohybrids for Photonic Devices. Advanced Materials, 2010, 22, 1635-1639.	11.1	112
29	Engineering the Low Coordinated Pt Single Atom to Achieve the Superior Electrocatalytic Performance toward Oxygen Reduction. Small, 2020, 16, e2003096.	5.2	110
30	Electronic structure of possible 3d `heavy-fermion' compound. Journal of Physics Condensed Matter, 1998, 10, L119-L126.	0.7	108
31	Pt–Au–Co Alloy Electrocatalysts Demonstrating Enhanced Activity and Durability toward the Oxygen Reduction Reaction. ACS Catalysis, 2015, 5, 1513-1524.	5.5	106
32	Pt/Pd Single-Atom Alloys as Highly Active Electrochemical Catalysts and the Origin of Enhanced Activity. ACS Catalysis, 2019, 9, 9350-9358.	5.5	106
33	Chemical and biological integration of a mouldable bioactive ceramic material capable of forming apatite in vivo in teeth. Biomaterials, 2004, 25, 2781-2787.	5.7	105
34	Tunable Syngas Production from CO ₂ and H ₂ O in an Aqueous Photoelectrochemical Cell. Angewandte Chemie - International Edition, 2016, 55, 14262-14266.	7.2	105
35	In Situ Liquid Cell TEM Study of Morphological Evolution and Degradation of Pt–Fe Nanocatalysts During Potential Cycling. Journal of Physical Chemistry C, 2014, 118, 22111-22119.	1.5	103
36	Bonding and structure of a reconstructed (001) surface of SrTiO3 from TEM. Nature, 2012, 490, 384-387.	13.7	102

#	Article	IF	CITATIONS
37	Mapping Bright and Dark Modes in Gold Nanoparticle Chains using Electron Energy Loss Spectroscopy Nano Letters, 2014, 14, 3799-3808.	4.5	100
38	High Efficiency Solar-to-Hydrogen Conversion on a Monolithically Integrated InGaN/GaN/Si Adaptive Tunnel Junction Photocathode. Nano Letters, 2015, 15, 2721-2726.	4.5	98
39	Can magneto-plasmonic nanohybrids efficiently combine photothermia with magnetic hyperthermia?. Nanoscale, 2015, 7, 18872-18877.	2.8	97
40	Strained Lattice with Persistent Atomic Order in Pt ₃ Fe ₂ Intermetallic Core–Shell Nanocatalysts. ACS Nano, 2013, 7, 6103-6110.	7.3	95
41	Engineering the Carrier Dynamics of InGaN Nanowire White Light-Emitting Diodes by Distributed p-AlGaN Electron Blocking Layers. Scientific Reports, 2015, 5, 7744.	1.6	93
42	Highly efficient binary copperâ~'iron catalyst for photoelectrochemical carbon dioxide reduction toward methane. Proceedings of the National Academy of Sciences of the United States of America, 2020, 117, 1330-1338.	3.3	93
43	Intracellular Biodegradation of Ag Nanoparticles, Storage in Ferritin, and Protection by a Au Shell for Enhanced Photothermal Therapy. ACS Nano, 2018, 12, 6523-6535.	7.3	91
44	High-resolution EELS study of the vacancy-doped metal/insulator system, Nd1â^'xTiO3, to 0.33 Journal of Solid State Chemistry, 2005, 178, 1008-1016.	1.4	90
45	Controlled Coalescence of AlGaN Nanowire Arrays: An Architecture for Nearly Dislocationâ€Free Planar Ultraviolet Photonic Device Applications. Advanced Materials, 2016, 28, 8446-8454.	11.1	90
46	Experimental and theoretical study of the electronic structure of Fe, Co, and Ni aluminides with theB2 structure. Physical Review B, 1996, 54, 1682-1691.	1.1	89
47	Synthesis of Metal Alloy Nanoparticles in Solution by Laser Irradiation of a Metal Powder Suspension. Journal of Physical Chemistry B, 2003, 107, 6920-6923.	1.2	87
48	Elemental mapping at the atomic scale using low accelerating voltages. Ultramicroscopy, 2010, 110, 926-934.	0.8	87
49	Microscopic Studies on Liquid Crystal Poly(3,3â€~Ââ€~â€~-dialkylquaterthiophene) Semiconductor. Macromolecules, 2004, 37, 8307-8312.	2.2	86
50	Dark-field transmission electron microscopy of cortical bone reveals details of extrafibrillar crystals. Journal of Structural Biology, 2014, 188, 240-248.	1.3	86
51	High Efficiency Si Photocathode Protected by Multifunctional GaN Nanostructures. Nano Letters, 2018, 18, 6530-6537.	4.5	83
52	Intergranular fracture in irradiated Inconel X-750 containing very high concentrations of helium and hydrogen. Journal of Nuclear Materials, 2015, 457, 165-172.	1.3	81
53	Three-Dimensional Quantum Confinement of Charge Carriers in Self-Organized AlGaN Nanowires: A Viable Route to Electrically Injected Deep Ultraviolet Lasers. Nano Letters, 2015, 15, 7801-7807.	4.5	80
54	AlN/h-BN Heterostructures for Mg Dopant-Free Deep Ultraviolet Photonics. Nano Letters, 2017, 17, 3738-3743.	4.5	78

#	Article	IF	CITATIONS
55	Quantification of the EELS nearâ€edge structures to study Mn doping in oxides. Journal of Microscopy, 1995, 180, 211-216.	0.8	75
56	A GaN:Sn nanoarchitecture integrated on a silicon platform for converting CO ₂ to HCOOH by photoelectrocatalysis. Energy and Environmental Science, 2019, 12, 2842-2848.	15.6	75
57	The role of aluminum distribution on the local corrosion resistance of the microstructure in a sand-cast AM50 alloy. Corrosion Science, 2013, 77, 151-163.	3.0	74
58	Silver Nanorice Structures: Oriented Attachment-Dominated Growth, High Environmental Sensitivity, and Real-Space Visualization of Multipolar Resonances. Chemistry of Materials, 2012, 24, 2339-2346.	3.2	71
59	Equilibrium and stability of phase-separating Au–Pt nanoparticles. Acta Materialia, 2008, 56, 5972-5983.	3.8	69
60	Cobalt-Free Nickel-Rich Positive Electrode Materials with a Core–Shell Structure. Chemistry of Materials, 2019, 31, 10150-10160.	3.2	69
61	Ternary Snâ€Tiâ€O Electrocatalyst Boosts the Stability and Energy Efficiency of CO ₂ Reduction. Angewandte Chemie - International Edition, 2020, 59, 12860-12867.	7.2	68
62	Quantitative Evaluation of Radiation Damage to Polyethylene Terephthalate by Soft X-rays and High-energy Electrons. Journal of Physical Chemistry B, 2009, 113, 1869-1876.	1.2	66
63	High-resolution observations of an amorphous layer and subsurface damage formed by femtosecond laser irradiation of silicon. Journal of Applied Physics, 2008, 103, .	1.1	63
64	Unassisted solar water splitting with 9.8% efficiency and over 100 h stability based on Si solar cells and photoelectrodes catalyzed by bifunctional Ni–Mo/Ni. Journal of Materials Chemistry A, 2019, 7, 2200-2209.	5.2	63
65	Towards calibration-invariant spectroscopy using deep learning. Scientific Reports, 2019, 9, 2126.	1.6	63
66	Selective Electrooxidation of Glycerol to Formic Acid over Carbon Supported Ni _{1–<i>x</i>} M _{<i>x</i>} (M = Bi, Pd, and Au) Nanocatalysts and Coelectrolysis of CO ₂ . ACS Applied Energy Materials, 2020, 3, 8725-8738.	2.5	63
67	Phase formation of CaAl2O4 from CaCO3–Al2O3 powder mixtures. Journal of the European Ceramic Society, 2008, 28, 747-756.	2.8	62
68	Molecular beam epitaxy growth of Al-rich AlGaN nanowires for deep ultraviolet optoelectronics. APL Materials, 2016, 4, .	2.2	62
69	GaP/GaAsP/GaP core–multishell nanowire heterostructures on (111) silicon. Nanotechnology, 2007, 18, 445304.	1.3	61
70	Structure and chemistry of the Si(111)/AlN interface. Applied Physics Letters, 2012, 100, .	1.5	61
71	Corrosion of engineering materials in a supercritical water cooled reactor: Characterization of oxide scales on Alloy 800H and stainless steel 316. Corrosion Science, 2015, 100, 222-230.	3.0	60
72	Photochemical Carbon Dioxide Reduction on Mg-Doped Ga(In)N Nanowire Arrays under Visible Light Irradiation. ACS Energy Letters, 2016, 1, 246-252.	8.8	60

#	Article	IF	CITATIONS
73	Three-dimensional investigation of cycling-induced microstructural changes in lithium-ion battery cathodes using focused ion beam/scanning electron microscopy. Journal of Power Sources, 2016, 306, 300-308.	4.0	60
74	Element Specific Monolayer Depth Profiling. Advanced Materials, 2014, 26, 6554-6559.	11.1	58
75	Nano- and Microstructure Engineering: An Effective Method for Creating High Efficiency Magnesium Silicide Based Thermoelectrics. ACS Applied Materials & Interfaces, 2016, 8, 34431-34437.	4.0	58
76	Selfâ€Assembled Functional DNA Superstructures as Highâ€Density and Versatile Recognition Elements for Printed Paper Sensors. Angewandte Chemie - International Edition, 2018, 57, 12440-12443.	7.2	58
77	Selective electroreduction of CO ₂ to formate on 3D [100] Pb dendrites with nanometer-sized needle-like tips. Journal of Materials Chemistry A, 2017, 5, 20747-20756.	5.2	56
78	Cross-sectional study of periodic surface structures on gallium phosphide induced by ultrashort laser pulse irradiation. Applied Physics Letters, 2008, 92, .	1.5	55
79	Nanocrystalline tungsten carbide (WC) synthesis/characterization and its possible application as a PEM fuel cell catalyst support. Electrochimica Acta, 2012, 61, 198-206.	2.6	55
80	Electroreduction of CO ₂ to formate on amine modified Pb electrodes. Journal of Materials Chemistry A, 2019, 7, 11272-11281.	5.2	55
81	Enhancement of resolution in core-loss and low-loss spectroscopy in a monochromated microscope. Ultramicroscopy, 2006, 106, 1091-1103.	0.8	54
82	Stable Hydrogen Storage Cycling in Magnesium Hydride, in the Range of Room Temperature to 300 °C, Achieved Using a New Bimetallic Cr-V Nanoscale Catalyst. Journal of Physical Chemistry C, 2012, 116, 3188-3199.	1.5	54
83	Scanning transmission electron microscopy investigation of the Si(111)/AlN interface grown by metalorganic vapor phase epitaxy. Applied Physics Letters, 2010, 97, .	1.5	52
84	Unraveling the Rapid Performance Decay of Layered High-Energy Cathodes: From Nanoscale Degradation to Drastic Bulk Evolution. ACS Nano, 2018, 12, 2708-2718.	7.3	52
85	Modification of Nickel Surfaces by Bismuth: Effect on Electrochemical Activity and Selectivity toward Glycerol. ACS Applied Materials & amp; Interfaces, 2020, 12, 15095-15107.	4.0	52
86	Dual-Site-Mediated Hydrogenation Catalysis on Pd/NiO: Selective Biomass Transformation and Maintenance of Catalytic Activity at Low Pd Loading. ACS Catalysis, 2020, 10, 5483-5492.	5.5	52
87	Surface-initiated atom transfer radical polymerization of polyhedral oligomeric silsesquioxane (POSS) methacrylate from flat silicon wafer. Polymer, 2006, 47, 1119-1123.	1.8	51
88	Highly Porous and Preferentially Oriented {100} Platinum Nanowires and Thin Films. Advanced Functional Materials, 2012, 22, 4172-4181.	7.8	51
89	Spatially resolved surface valence gradient and structural transformation of lithium transition metal oxides in lithium-ion batteries. Physical Chemistry Chemical Physics, 2016, 18, 29064-29075.	1.3	51
90	Electron Energy-Loss Spectroscopy of Multipolar Edge and Cavity Modes in Silver Nanosquares. ACS Photonics, 2016, 3, 428-433.	3.2	51

#	Article	IF	CITATIONS
91	Magnetoâ€Thermal Metrics Can Mirror the Longâ€Term Intracellular Fate of Magnetoâ€Plasmonic Nanohybrids and Reveal the Remarkable Shielding Effect of Gold. Advanced Functional Materials, 2017, 27, 1605997.	7.8	51
92	Ti4O7 supported Ru@Pt core–shell catalyst for CO-tolerance in PEM fuel cell hydrogen oxidation reaction. Applied Energy, 2013, 103, 507-513.	5.1	50
93	InGaN/Si Double-Junction Photocathode for Unassisted Solar Water Splitting. ACS Energy Letters, 2020, 5, 3741-3751.	8.8	49
94	Mechanism of Action of the Tungsten Dopant in LiNiO ₂ Positive Electrode Materials. Advanced Energy Materials, 2022, 12, .	10.2	49
95	Experimental evidence of nanometer-scale confinement of plasmonic eigenmodes responsible for hot spots in random metallic films. Physical Review B, 2013, 88, .	1.1	48
96	The cathodic behaviour of Al–Mn precipitates during atmospheric and saline aqueous corrosion of a sand-cast AM50 alloy. Corrosion Science, 2014, 83, 299-309.	3.0	47
97	Ultralow Loading and High-Performing Pt Catalyst for a Polymer Electrolyte Membrane Fuel Cell Anode Achieved by Atomic Layer Deposition. ACS Catalysis, 2019, 9, 5365-5374.	5.5	47
98	Sizeâ€Mediated Recurring Spinel Subâ€nanodomains in Li―and Mnâ€Rich Layered Cathode Materials. Angewandte Chemie - International Edition, 2020, 59, 14313-14320.	7.2	46
99	Uncovering the nature of electroactive sites in nano architectured dendritic Bi for highly efficient CO2 electroreduction to formate. Applied Catalysis B: Environmental, 2020, 274, 119031.	10.8	46
100	Surface-initiated atom transfer radical polymerization grafting of poly(2,2,2-trifluoroethyl) Tj ETQq0 0 0 rgBT /Ov	erlock 10 2.5	Tf 50 382 Td 45
101	Nucleation and growth of Si nanocrystals in an amorphousSiO2matrix. Physical Review B, 2006, 74, .	1.1	45
102	Strain relief and AlSb buffer layer morphology in GaSb heteroepitaxial films grown on Si as revealed by high-angle annular dark-field scanning transmission electron microscopy. Applied Physics Letters, 2011, 98, .	1.5	45
103	Supramolecular Functionalization of Single-Walled Carbon Nanotubes with Conjugated Polyelectrolytes and Their Patterning on Surfaces. Macromolecules, 2008, 41, 9869-9874.	2.2	44
104	A novel CO-tolerant PtRu core–shell structured electrocatalyst with Ru rich in core and Pt rich in shell for hydrogen oxidation reaction and its implication in proton exchange membrane fuel cell. Journal of Power Sources, 2011, 196, 9117-9123.	4.0	44
105	Tracking the corrosion of magnesium sand cast AM50 alloy in chloride environments. Corrosion Science, 2013, 75, 114-122.	3.0	43
106	Asymmetric Silver "Nanocarrot―Structures: Solution Synthesis and Their Asymmetric Plasmonic Resonances. Journal of the American Chemical Society, 2013, 135, 9616-9619.	6.6	43
107	Oxidation of Fe Nanoparticles Embedded in Single-Walled Carbon Nanotubes by Exposure to a Bright Flash of White Light. Nano Letters, 2002, 2, 1277-1280.	4.5	42
108	Atomic scale real-space mapping of holes in YBa2Cu3O6+Ĵ′. Nature Communications, 2014, 5, 4275.	5.8	42

#	Article	IF	CITATIONS
109	Selective area epitaxy of AlGaN nanowire arrays across nearly the entire compositional range for deep ultraviolet photonics. Optics Express, 2017, 25, 30494.	1.7	42
110	Electron Energy Loss Spectroscopy Investigation into Symmetry in Gold Trimer and Tetramer Plasmonic Nanoparticle Structures. ACS Nano, 2016, 10, 8552-8563.	7.3	41
111	Molecular beam epitaxial growth and characterization of Al(Ga)N nanowire deep ultraviolet light emitting diodes and lasers. Journal Physics D: Applied Physics, 2016, 49, 364006.	1.3	41
112	Epitaxial thin films of multiferroic Bi ₂ FeCrO ₆ with <i>B</i> -site cationic order. Journal of Materials Research, 2007, 22, 2102-2110.	1.2	39
113	Synthesis and Electrophoretic Deposition of Single-Walled Carbon Nanotube Complexes with a Conjugated Polyelectrolyte. Chemistry of Materials, 2010, 22, 2741-2749.	3.2	39
114	Formation of the Ternary Complex Hydride Mg ₂ FeH ₆ from Magnesium Hydride (β-MgH ₂) and Iron: An Electron Microscopy and Energy-Loss Spectroscopy Study. Journal of Physical Chemistry C, 2012, 116, 25701-25714.	1.5	39
115	Atomic Resolution Coordination Mapping in Ca ₂ FeCoO ₅ Brownmillerite by Spatially Resolved Electron Energy-Loss Spectroscopy. Chemistry of Materials, 2012, 24, 1904-1909.	3.2	39
116	High-Efficiency InGaN/GaN Dot-in-a-Wire Red Light-Emitting Diodes. IEEE Photonics Technology Letters, 2012, 24, 321-323.	1.3	38
117	Electrochemical Valorization of Glycerol on Ni-Rich Bimetallic NiPd Nanoparticles: Insight into Product Selectivity Using in Situ Polarization Modulation Infrared-Reflection Absorption Spectroscopy. ACS Sustainable Chemistry and Engineering, 2019, 7, 14425-14434.	3.2	38
118	Multiple-interface coupling effects in local electron-energy-loss measurements of band gap energies. Physical Review B, 2007, 76, .	1.1	37
119	Self-Constructed Multiple Plasmonic Hotspots on an Individual Fractal to Amplify Broadband Hot Electron Generation. ACS Nano, 2021, 15, 10553-10564.	7.3	37
120	Imaging, Core-Loss, and Low-Loss Electron-Energy-Loss Spectroscopy Mapping in Aberration-Corrected STEM. Microscopy and Microanalysis, 2010, 16, 416-424.	0.2	36
121	Toward 10 meV Electron Energy-Loss Spectroscopy Resolution for Plasmonics. Microscopy and Microanalysis, 2014, 20, 767-778.	0.2	36
122	Visualizing biointerfaces in three dimensions: electron tomography of the bone–hydroxyapatite interface. Journal of the Royal Society Interface, 2010, 7, 1497-1501.	1.5	35
123	Iron oxyhydroxide colloid formation by gamma-radiolysis. Physical Chemistry Chemical Physics, 2011, 13, 7198.	1.3	35
124	Resonant optical excitations in complementary plasmonic nanostructures. Optics Express, 2012, 20, 6968.	1.7	34
125	Electron energy loss spectroscopy of interfacial layer formation in Gd2O3 films deposited directly on Si(001). Journal of Applied Physics, 2002, 91, 2921-2928.	1.1	33
126	Strain fields around dislocation arrays in a Σ9 silicon bicrystal measured by scanning transmission electron microscopy. Philosophical Magazine, 2013, 93, 1250-1267.	0.7	33

#	Article	IF	CITATIONS
127	Self-Similarity of Plasmon Edge Modes on Koch Fractal Antennas. ACS Nano, 2017, 11, 11240-11249.	7.3	33
128	Impact of a Titanium-Based Surface Coating Applied to Li[Ni _{0.5} Mn _{0.3} Co _{0.2}]O ₂ on Lithium-Ion Cell Performance. ACS Applied Energy Materials, 2018, 1, 7052-7064.	2.5	33
129	Probing the performance of structurally controlled platinum-cobalt bimetallic catalysts for selective hydrogenation of cinnamaldehyde. Journal of Catalysis, 2020, 388, 164-170.	3.1	33
130	Atomic Ordering in InGaN Alloys within Nanowire Heterostructures. Nano Letters, 2015, 15, 6413-6418.	4.5	32
131	2D strain mapping using scanning transmission electron microscopy Moiré interferometry and geometrical phase analysis. Ultramicroscopy, 2018, 187, 1-12.	0.8	32
132	Growth mechanisms of GaSb heteroepitaxial films on Si with an AlSb buffer layer. Journal of Applied Physics, 2013, 114, 113101.	1.1	31
133	Magnetocaloric effect in Ni-Mn-Ga thin films under concurrent magnetostructural and Curie transitions. Journal of Applied Physics, 2011, 110, 013910.	1.1	30
134	Lattice distortions and octahedral rotations in epitaxially strained LaNiO3/LaAlO3 superlattices. Applied Physics Letters, 2014, 104, .	1.5	30
135	Atomically resolved EELS mapping of the interfacial structure of epitaxially strained <mml:math xmlns:mml="http://www.w3.org/1998/Math/MathML"><mml:msub><mml:mrow><mml:mi mathvariant="normal">LaNiO</mml:mi </mml:mrow><mml:mn>3</mml:mn></mml:msub><ml:mo>/mathvariant="normal">LaAIO<mml:mn>3</mml:mn>super</ml:mo></mml:math 		നട ൾ < mml:n
136	Physical Review 8, 2014, 90, . Epitaxially stabilized thin films of Îμ-Fe2O3 (001) grown on YSZ (100). Scientific Reports, 2017, 7, 3712.	1.6	30
137	Artificial Solids by Design: Assembly and Electron Microscopy Study of Nanosheet-Derived Heterostructures. Chemistry of Materials, 2013, 25, 4892-4900.	3.2	29
138	Local Hydrogen Fluxes Correlated to Microstructural Features of a Corroding Sand Cast AM50 Magnesium Alloy. Journal of the Electrochemical Society, 2014, 161, C557-C564.	1.3	29
139	Plasmonic Coupling of Multipolar Edge Modes and the Formation of Gap Modes. ACS Photonics, 2017, 4, 1558-1565.	3.2	29
140	GaN nanowires as a reusable photoredox catalyst for radical coupling of carbonyl under blacklight irradiation. Chemical Science, 2020, 11, 7864-7870.	3.7	29
141	Biaxial ZnOâ^'ZnS Nanoribbon Heterostructures. Journal of Physical Chemistry C, 2009, 113, 4755-4757.	1.5	28
142	Microscopic investigation of single-crystal diamond following ultrafast laser irradiation. Applied Physics A: Materials Science and Processing, 2011, 103, 185-192.	1.1	28
143	Synthesis of Cu–Pd alloy thin films by co-electrodeposition. Electrochimica Acta, 2011, 56, 7397-7403.	2.6	28
144	Evidence of Eu2+ 4 <i>f</i> electrons in the valence band spectra of EuTiO3 and EuZrO3. Journal of Applied Physics, 2012, 112, .	1.1	28

#	Article	IF	CITATIONS
145	Ionomer content optimization in nickel-iron-based anodes with and without ceria for anion exchange membrane water electrolysis. Journal of Power Sources, 2021, 514, 230563.	4.0	28
146	<i>In situ</i> controlled modification of the helium density in single helium-filled nanobubbles. Journal of Applied Physics, 2014, 115, .	1.1	27
147	Europium-doped ZnO nanosponges – controlling optical properties and photocatalytic activity. Journal of Materials Chemistry C, 2019, 7, 3909-3919.	2.7	27
148	Broken Band Alignment in EuS-CdS Nanoheterostructures. Chemistry of Materials, 2011, 23, 181-187.	3.2	25
149	Synthesis of Pd and Nb–doped TiO2 composite supports and their corresponding Pt–Pd alloy catalysts by a two-step procedure for the oxygen reduction reaction. Journal of Power Sources, 2013, 221, 232-241.	4.0	25
150	Surface Segregation of Fe in Pt–Fe Alloy Nanoparticles: Its Precedence and Effect on the Orderedâ€Phase Evolution during Thermal Annealing. ChemCatChem, 2015, 7, 3655-3664.	1.8	25
151	Localized Corrosion Behavior of AZ31B Magnesium Alloy with an Electrodeposited Poly(3,4-Ethylenedioxythiophene) Coating. Journal of the Electrochemical Society, 2015, 162, C536-C544.	1.3	25
152	Effects of bond character on the electronic structure of brownmillerite-phase oxides, Ca2B′xFe2â^'xO5 (B′ = Al, Ga): an X-ray absorption and electron energy loss spectroscopic study. Journal of Materials Chemistry, 2009, 19, 9213.	6.7	24
153	Three-Dimensional Atomic Structure of Metastable Nanoclusters in Doped Semiconductors. Physical Review Letters, 2011, 107, 186104.	2.9	24
154	Interplay of strain and indium incorporation in InGaN/GaN dot-in-a-wire nanostructures by scanning transmission electron microscopy. Nanotechnology, 2015, 26, 344002.	1.3	24
155	Preparation of Ni-g-polymer core–shell nanoparticles by surface-initiated atom transfer radical polymerization. Polymer, 2009, 50, 4293-4298.	1.8	23
156	Bone Response to Freeâ€Form Fabricated Hydroxyapatite and Zirconia Scaffolds: A Transmission Electron Microscopy Study in the Human Maxilla. Clinical Implant Dentistry and Related Research, 2012, 14, 461-469.	1.6	23
157	Cu ₂ Se and Cu Nanocrystals as Local Sources of Copper in Thermally Activated <i>In Situ</i> Cation Exchange. ACS Nano, 2016, 10, 2406-2414.	7.3	23
158	Liquid Cell Transmission Electron Microscopy Sheds Light on The Mechanism of Palladium Electrodeposition. Langmuir, 2019, 35, 862-869.	1.6	23
159	Unveiling the role of surface, size, shape and defects of iron oxide nanoparticles for theranostic applications. Nanoscale, 2021, 13, 14552-14571.	2.8	23
160	Evaluating focused ion beam and ultramicrotome sample preparation for analytical microscopies of the cathode layer of a polymer electrolyte membrane fuel cell. Journal of Power Sources, 2016, 312, 23-35.	4.0	22
161	Review—Multifunctional Separators: A Promising Approach for Improving the Durability and Performance of Li-Ion Batteries. Journal of the Electrochemical Society, 2019, 166, A5369-A5377.	1.3	22
162	Analytical Electron Microscopy Studies of Lithium Aluminum Hydrides with Ti- and V-Based Additives. Journal of Physical Chemistry B, 2005, 109, 4350-4356.	1.2	21

#	Article	IF	CITATIONS
163	Structural and transport properties of epitaxial niobium-doped BaTiO3 films. Applied Physics Letters, 2008, 93, 192114.	1.5	21
164	Self-activated reversibility in the magnetically induced reorientation of martensitic variants in ferromagnetic Ni-Mn-Ga films. Physical Review B, 2010, 81, .	1.1	21
165	The role of vicinal silicon surfaces in the formation of epitaxial twins during the growth of III-V thin films. Journal of Applied Physics, 2011, 110, .	1.1	21
166	A Vacancy-Disordered, Oxygen-Deficient Perovskite with Long-Range Magnetic Ordering: Local and Average Structures and Magnetic Properties of Sr ₂ Fe _{1.5} Cr _{0.5} O ₅ . Inorganic Chemistry, 2012, 51, 2638-2644.	1.9	21
167	Solute Segregation During Ferrite Growth: Solute/Interphase and Substitutional/Interstitial Interactions. Jom, 2016, 68, 1329-1334.	0.9	21
168	Compositional and Morphological Changes of Ordered Pt _{<i>x</i>} Fe _{<i>y</i>} /C Oxygen Electroreduction Catalysts. ChemCatChem, 2013, 5, 1449-1460.	1.8	20
169	Analytical electron microscopy of a crack tip extracted from a stressed Alloy 800 sample exposed to an acid sulfate environment. Micron, 2014, 61, 62-69.	1.1	20
170	Enhanced figure of merit in Mg ₂ Si _{0.877} Ge _{0.1} Bi _{0.023} /multi wall carbon nanotube nanocomposites. RSC Advances, 2015, 5, 65328-65336.	1.7	20
171	Real-space localization and quantification of hole distribution in chain-ladder Sr ₃ Ca ₁₁ Cu ₂₄ O ₄₁ superconductor. Science Advances, 2016, 2, e1501652.	4.7	20
172	Targeting low-cost type-II heterostructures: Synthesis, structure and photoreactivity. Journal of Alloys and Compounds, 2017, 698, 944-956.	2.8	20
173	Efficient Graphene Production by Combined Bipolar Electrochemical Intercalation and High-Shear Exfoliation. ACS Omega, 2017, 2, 6492-6499.	1.6	20
174	Nanoscale mechanism of the stabilization of nanoporous gold by alloyed platinum. Nanoscale, 2018, 10, 4904-4912.	2.8	20
175	Seeing structures and measuring properties with transmission electron microscopy images: A simple combination to study size effects in nanoparticle systems. Applied Physics Letters, 2009, 94, .	1.5	19
176	Local structure and thermoelectric properties of Mg2Si0.977â^'Ge Bi0.023 (0.1 ⩽x⩽ 0.4). Journal of Alloys and Compounds, 2015, 644, 249-255.	⁵ 2.8	19
177	Synthesis and structural evolution of Pt nanotubular skeletons: revealing the source of the instability of nanostructured electrocatalysts. Journal of Materials Chemistry A, 2015, 3, 12663-12671.	5.2	19
178	Effect of Silicon Carbide Nanoparticles on the Grain Boundary Segregation and Thermoelectric Properties of Bismuth Doped Mg2Si0.7Ge0.3. Journal of Electronic Materials, 2016, 45, 6052-6058.	1.0	19
179	Phosphorus oxide gate dielectric for black phosphorus field effect transistors. Applied Physics Letters, 2018, 112, .	1.5	19
180	Surface modification and cathodic electrophoretic deposition of ceramic materials and composites using celestine blue dye. RSC Advances, 2014, 4, 29652.	1.7	18

#	Article	IF	CITATIONS
181	Multivariate-aided mapping of rare-earth partitioning in a wrought magnesium alloy. Scripta Materialia, 2016, 124, 174-178.	2.6	18
182	Investigating the Removal of Layered Double Hydroxides in [Ni _{0.80} Co _{0.15}] _{0.95-x} Al _{0.05+x} (OH) ₂ (x = 0,) Tj	eTiQaq00() rg&T /Overl
183	Structural and multiferroic properties of epitaxial γ-Fe ₂ O ₃ –BiFeO ₃ /Bi _{3.25} La _{0.75} Ti _{3bi-layers. Journal Physics D: Applied Physics, 2008, 41, 112002.}	ba@	>12ҡ/sub>co
184	Metallic and Semiconducting Single-Walled Carbon Nanotubes: Differentiating Individual SWCNTs by Their Carbon 1s Spectra. ACS Nano, 2012, 6, 10965-10972.	7.3	17
185	Mapping defects in a carbon nanotube by momentum transfer dependent electron energy loss spectromicroscopy. Ultramicroscopy, 2012, 113, 158-164.	0.8	17
186	Sub-Ã¥ngstrom Experimental Validation of Molecular Dynamics for Predictive Modeling of Extended Defect Structures in Si. Physical Review Letters, 2013, 110, 166102.	2.9	17
187	Real-space mapping of electronic orbitals. Ultramicroscopy, 2017, 177, 26-29.	0.8	17
188	A Low-Cost Instrument for Dry Particle Fusion Coating of Advanced Electrode Material Particles at the Laboratory Scale. Journal of the Electrochemical Society, 2020, 167, 110509.	1.3	17
189	Electron energy loss spectroscopy studies of the amorphous to crystalline transition in FeF3. Journal of Applied Physics, 1999, 86, 2499-2504.	1.1	16
190	Coexistence of A―and B‧ite Vacancy Compensation in Laâ€Doped Sr _{1â^'<i>x</i>} Ba <i>_x</i> TiO ₃ . Journal of the American Ceramic Society, 2010, 93, 2903-2908.	1.9	16
191	Atomic-resolution study of polarity reversal in GaSb grown on Si by scanning transmission electron microscopy. Journal of Applied Physics, 2012, 112, .	1.1	16
192	Atomic structure and bonding of the interfacial bilayer between Au nanoparticles and epitaxially regrown MgAl2O4 substrates. Applied Physics Letters, 2014, 105, .	1.5	16
193	In Liquid Observation and Quantification of Nucleation and Growth of Gold Nanostructures Using in Situ Transmission Electron Microscopy. Journal of Physical Chemistry C, 2017, 121, 7435-7441.	1.5	16
194	Efficient Nitrogen Fixation Catalyzed by Gallium Nitride Nanowire Using Nitrogen and Water. IScience, 2019, 17, 208-216.	1.9	16
195	Volume fraction measurement of dispersoids in a thin foil by parallel energyâ€loss spectroscopy: development and assessment of the technique. Journal of Microscopy, 1995, 180, 217-229.	0.8	15
196	Locating La atoms in epitaxial Bi3.25La0.75Ti3O12 films through atomic resolution electron energy loss spectroscopy mapping. Applied Physics Letters, 2009, 95, .	1.5	15
197	Imaging High-Energy Electrons Propagating in a Crystal. Physical Review Letters, 2011, 106, 160802.	2.9	15
198	Probing bonding and electronic structure at atomic resolution with spectroscopic imaging. MRS Bulletin, 2012, 37, 21-28.	1.7	15

#	Article	IF	CITATIONS
199	Oxygen 1 <mml:math xmins:mml="http://www.w3.org/1998/Math/Math/Math/Math/Math/Math/Math/Math</td"><td>1.1</td><td>15</td></mml:math>	1.1	15
200	Synthesis and Optical Properties of Linker-Free TiO ₂ /CdSe Nanorods. Journal of Physical Chemistry C, 2014, 118, 3347-3358.	1.5	15
201	Primary Oxide Latent Storage and Spillover Enabling Electrocatalysts with Reversible Oxygen Electrode Properties and the Alterpolar Revertible (PEMFC versus WE) Cell. Journal of Physical Chemistry C, 2014, 118, 8723-8746.	1.5	15
202	An In0.5Ga0.5N nanowire photoanode for harvesting deep visible light photons. APL Materials, 2016, 4, .	2.2	15
203	Temperature-dependent high energy-resolution EELS of ferroelectric and paraelectric <mml:math xmlns:mml="http://www.w3.org/1998/Math/MathML"><mml:msub><mml:mi>BaTiO</mml:mi><mml:mn>3Physical Review B, 2016, 93, .</mml:mn></mml:msub></mml:math 	ıml:mb.ai.> <	/mmlɪ ธ ารub> </td
204	Revealing the Structure Evolution of Heterogeneous Pd Catalyst in Suzuki Reaction via the Identical Location Transmission Electron Microscopy. ACS Nano, 2021, 15, 8621-8637.	7.3	15
205	Advances in ultrahigh-energy resolution EELS: phonons, infrared plasmons and strongly coupled modes. Microscopy (Oxford, England), 2022, 71, i174-i199.	0.7	15
206	Highâ€Voltage Induced Surface and Intragranular Structural Evolution of Niâ€Rich Layered Cathode. Small, 2022, 18, e2200627.	5.2	15
207	Changes in the iron whiteâ€line ratio in the electron energyâ€loss spectrum of ironâ€copper multilayers. Journal of Microscopy, 1995, 180, 288-293.	0.8	14
208	Synthesis of hierarchical structured porous MoS ₂ /SiO ₂ microspheres by ultrasonic spray pyrolysis. Canadian Journal of Chemical Engineering, 2012, 90, 330-335.	0.9	14
209	AuPt Alloy on TiO ₂ : A Selective and Durable Catalyst for <scp>l</scp> â€Sorbose Oxidation to 2â€Ketoâ€Gulonic Acid. ChemSusChem, 2015, 8, 4189-4194.	3.6	14
210	Ablation and structural changes induced in InP surfaces by single 10 fs laser pulses in air. Journal of Applied Physics, 2009, 106, 074907.	1,1	13
211	Thermoelectric properties of A0.05Mo3Sb5.4Te1.6 (A=Mn, Fe, Co, Ni). Journal of Alloys and Compounds, 2010, 504, 314-319.	2.8	13
212	Structure, ordering, and surfaces of Pt–Fe alloy catalytic nanoparticles from quantitative electron microscopy and X-ray diffraction. Nanoscale, 2012, 4, 7273.	2.8	13
213	Theory, Substantiation, and Properties of Novel Reversible Electrocatalysts for Oxygen Electrode Reactions. Journal of Physical Chemistry C, 2015, 119, 11267-11285.	1.5	13
214	Biomimetic design of monolithic fuel cell electrodes with hierarchical structures. Nano Energy, 2016, 20, 57-67.	8.2	13
215	Nanoscale analysis of structural and chemical changes in aged hybrid Pt/NbO x /C fuel cell catalysts. Journal of Power Sources, 2017, 356, 140-152.	4.0	13
216	PtRu Alloy Nanoparticles I. Physicochemical Characterizations of Structures Formed as a Function of the Type of Deposition and Their Evolutions on Annealing. Journal of Physical Chemistry C, 2017, 121, 23104-23119.	1.5	13

#	Article	IF	CITATIONS
217	Electrochemical promotion of Bi-metallic Ni9Pd core double-shell nanoparticles for complete methane oxidation. Journal of Catalysis, 2019, 374, 127-135.	3.1	13
218	Remarkably Stable Nickel Hydroxide Nanoparticles for Miniaturized Electrochemical Energy Storage. ACS Applied Energy Materials, 2020, 3, 7294-7305.	2.5	13
219	Sub-4 nm Nanodiamonds from Graphene-Oxide and Nitrated Polycyclic Aromatic Hydrocarbons at 423 K. ACS Nano, 2021, 15, 17392-17400.	7.3	13
220	Direct observation of anti-phase boundaries in heteroepitaxy of GaSb thin films grown on Si(001) by transmission electron microscopy. Journal of Applied Physics, 2012, 112, 074306.	1.1	12
221	Thermodynamically destabilized hydride formation in "bulk―Mg–AlTi multilayers for hydrogen storage. Physical Chemistry Chemical Physics, 2013, 15, 16432.	1.3	12
222	Corrosion Product Formation Monitored Using the Feedback Mode of Scanning Electrochemical Microscopy with Carbon Microelectrodes. Journal of the Electrochemical Society, 2015, 162, C677-C683.	1.3	12
223	Tunable Syngas Production from CO ₂ and H ₂ O in an Aqueous Photoelectrochemical Cell. Angewandte Chemie, 2016, 128, 14474-14478.	1.6	12
224	The Effect of Interdiffusion on the Properties of Lithium-Rich Core-Shell Cathodes. Journal of the Electrochemical Society, 2016, 163, A2841-A2848.	1.3	12
225	Structural origin of the high-performance light-emitting InGaN/AlGaN quantum disks. Nanoscale, 2019, 11, 8994-8999.	2.8	12
226	Preformed Au colloidal nanoparticles immobilised on NiO as highly efficient heterogeneous catalysts for reduction of 4-nitrophenol to 4-aminophenol. Journal of Environmental Chemical Engineering, 2019, 7, 103381.	3.3	12
227	Sampling optimization of Moiré geometrical phase analysis for strain characterization in scanning transmission electron microscopy. Ultramicroscopy, 2020, 209, 112858.	0.8	12
228	The performance evaluation of direct detection electron energy-loss spectroscopy at 200ÅkV and 80ÅkV accelerating voltages. Ultramicroscopy, 2020, 212, 112942.	0.8	12
229	Hierarchical Plasmon Resonances in Fractal Structures. ACS Photonics, 2020, 7, 1246-1254.	3.2	12
230	Influence of Pd and Au on electrochemical valorization of glycerol over Ni-rich surfaces. Journal of Catalysis, 2021, 396, 1-13.	3.1	12
231	Investigation of the electronic structure of the cubic spinel Cu1.2Mn1.8O4 using electron energy loss spectroscopy. Solid State Ionics, 2008, 179, 718-724.	1.3	11
232	Atomic-level 2-dimensional chemical mapping and imaging of individual dopants in a phosphor crystal. Physical Chemistry Chemical Physics, 2013, 15, 11420.	1.3	11
233	Studying Tomorrow's Materials Today: Insights with Quantitative STEM, EELS. Microscopy and Microanalysis, 2014, 20, 78-79.	0.2	11
234	Diols Production From Glycerol Over Pt-Based Catalysts: On the Role Played by the Acid Sites of the Support. Catalysis Letters, 2017, 147, 2523-2533.	1.4	11

#	Article	IF	CITATIONS
235	2D Antimony–Arsenic Alloys. Small, 2020, 16, 1906540.	5.2	11
236	Resonant Optical Antennas with Atomic-Sized Tips and Tunable Gaps Achieved by Mechanical Actuation and Electrical Control. Nano Letters, 2020, 20, 4346-4353.	4.5	11
237	Highly Active Nickel–Iron Nanoparticles With and Without Ceria for the Oxygen Evolution Reaction. Electrocatalysis, 2021, 12, 605-618.	1.5	11
238	Single atomic layer detection of Ca and defect characterization of Bi-2212 with EELS in HA-ADF STEM. Ultramicroscopy, 2006, 106, 1076-1081.	0.8	10
239	Electron inelastic scattering and anisotropy: The two-dimensional point of view. Ultramicroscopy, 2006, 106, 1082-1090.	0.8	10
240	STEM HAADF Tomography of Molybdenum Disulfide with Mesoporous Structure. ChemCatChem, 2011, 3, 999-1003.	1.8	10
241	Tilted epitaxy on (211)-oriented substrates. Applied Physics Letters, 2013, 102, 132103.	1.5	10
242	Homogenization Study of the Effects of Cycling on the Electronic Conductivity of Commercial Lithium-Ion Battery Cathodes. Journal of Physical Chemistry C, 2015, 119, 12199-12208.	1.5	10
243	High resolution transmission electron microscopy (TEM), energy-dispersive X-ray spectroscopy (EDS) and X-ray diffraction studies of nanocrystalline manganese borohydride (Mn(BH4)2) after mechano-chemical synthesis and thermal dehydrogenation. Acta Materialia, 2015, 100, 392-400.	3.8	10
244	Heterogeneous diamond phases in compressed graphite studied by electron energy-loss spectroscopy. Diamond and Related Materials, 2016, 64, 190-196.	1.8	10
245	Amorphous Ni-Based Nanoparticles for Alkaline Oxygen Evolution. ACS Applied Nano Materials, 2020, 3, 10522-10530.	2.4	10
246	Piezoresponse force microscopy and magnetic force microscopy characterization of γ-Fe2O3–BiFeO3 nanocomposite/Bi3.25La0.75Ti3O12 multiferroic bilayers. Journal of Magnetism and Magnetic Materials, 2009, 321, 1799-1802.	1.0	9
247	(100) MgAl2O4 as a lattice-matched substrate for the epitaxial thin film deposition of the relaxor ferroelectric PMN-PT. Applied Physics A: Materials Science and Processing, 2010, 98, 187-194.	1.1	9
248	Cross-sectional study of femtosecond laser bulk modification ofÂcrystalline α-quartz. Applied Physics A: Materials Science and Processing, 2010, 98, 849-853.	1.1	9
249	Evidence for an equilibrium epitaxial complexion at the Au-MgAl2O4 interface. Applied Physics Letters, 2015, 107, .	1.5	9
250	Coupling of bias-induced crystallographic shear planes with charged domain walls in ferroelectric oxide thin films. Physical Review B, 2016, 94, .	1.1	9
251	Effect of water vapour partial pressure on the chromia (Cr ₂ O ₃)-based scale stability. Canadian Metallurgical Quarterly, 2018, 57, 89-98.	0.4	9
252	Elucidating the Li-Ion Battery Performance Benefits Enabled by Multifunctional Separators. ACS Applied Energy Materials, 2018, 1, 1878-1882.	2.5	9

#	Article	IF	CITATIONS
253	Carving Plasmon Modes in Silver Sierpiński Fractals. ACS Photonics, 2019, 6, 2974-2984.	3.2	9
254	Sizeâ€Mediated Recurring Spinel Subâ€nanodomains in Li―and Mnâ€Rich Layered Cathode Materials. Angewandte Chemie, 2020, 132, 14419-14426.	1.6	9
255	Electronic Structure and Elastic Properties of Strongly Correlated Metal Oxides from First Principles: LSDA + U, SIC-LSDA and EELS Study of UO2 and NiO. , 1998, 166, 429.		9
256	Deciphering the Interaction of Single-Phase La _{0.3} Sr _{0.7} Fe _{0.7} Cr _{0.3} O _{3-δ} with CO ₂ /CO Environments for Application in Reversible Solid Oxide Cells. ACS Applied Materials & amp; Interfaces, 2022, 14, 13388-13399.	4.0	9
257	Interface Segregation and Nitrogen Measurement in Fe–Mn–N Steel by Atom Probe Tomography. Microscopy and Microanalysis, 2017, 23, 385-395.	0.2	8
258	Bulk Immiscibility at the Edge of the Nanoscale. ACS Nano, 2017, 11, 10984-10991.	7.3	8
259	The 3D Nanoscale Evolution of Platinum–Niobium Oxide Fuel Cell Catalysts via Identical Location Electron Tomography. Particle and Particle Systems Characterization, 2017, 34, 1700051.	1.2	8
260	Advances in nanoscale characterization of refined nanoporous gold. Electrochimica Acta, 2018, 283, 611-618.	2.6	8
261	Revealing the Effects of Trace Oxygen Vacancies on Improper Ferroelectric Manganite with In Situ Biasing. Advanced Electronic Materials, 2019, 5, 1800827.	2.6	8
262	Ternary Snâ€īiâ€O Electrocatalyst Boosts the Stability and Energy Efficiency of CO 2 Reduction. Angewandte Chemie, 2020, 132, 12960-12967.	1.6	8
263	Electronic Structure and Elastic Properties of Strongly Correlated Metal Oxides from First Principles: LSDA + U, SIC-LSDA and EELS Study of UO2 and NiO. , 1998, 166, 429.		8
264	Structure and morphology of Pt3Sc alloy thin film prepared by pulsed laser deposition. Thin Solid Films, 2012, 524, 127-132.	0.8	7
265	Pnictogens Allotropy and Phase Transformation during van der Waals Growth. Nano Letters, 2020, 20, 8258-8266.	4.5	7
266	Electron energy-loss spectroscopy of surface plasmon activity in wrinkled gold structures. Journal of Chemical Physics, 2020, 153, 224703.	1.2	7
267	Strain-free ultrathin AlN epilayers grown directly on sapphire by high-temperature molecular beam epitaxy. Applied Physics Letters, 2020, 116, .	1.5	7
268	Morphology alteration of nickel microstructures for glycerol electrooxidation. Journal of Catalysis, 2021, 404, 348-361.	3.1	7
269	Correlating the mechanical strength of positive electrode material particles to their capacity retention. Cell Reports Physical Science, 2022, 3, 100714.	2.8	7
270	Plasmon coupling and finite size effects in metallic multilayers. Journal of Microscopy, 1997, 187, 184-192.	0.8	6

#	Article	IF	CITATIONS
271	Quantitative compositional analysis and strain study of InAs quantum wires with InGaAlAs barrier layers. Journal of Applied Physics, 2009, 105, .	1.1	6
272	Lattice-registered growth of GaSb on Si (211) with molecular beam epitaxy. Journal of Applied Physics, 2012, 112, .	1.1	6
273	Direct observation of indium precipitates in silicon following high dose ion implantation. Semiconductor Science and Technology, 2013, 28, 125012.	1.0	6
274	Atomic-scale Ge diffusion in strained Si revealed by quantitative scanning transmission electron microscopy. Physical Review B, 2013, 87, .	1.1	6
275	Modeling and experimental characterization of stepped and v-shaped {311} defects in silicon. Journal of Applied Physics, 2014, 115, 143514.	1.1	6
276	Growth and kinetic Monte Carlo simulation of InAs quantum wires on vicinal substrates. Journal of Crystal Growth, 2015, 412, 87-94.	0.7	6
277	Damage behavior and atomic migration in MgAl 2 O 4 under an 80 keV scanning focused probe in a STEM. Micron, 2015, 68, 141-145.	1.1	6
278	Characterization of Localized Filament Corrosion Products at the Anodic Head on a Model Mg-Zn-Zr Alloy Surface. Corrosion, 2017, 73, 518-525.	0.5	6
279	Silicon effects on the wet oxidation of type 310 stainless steel. Corrosion Science, 2018, 143, 376-389.	3.0	6
280	Deposition and morphological evolution of nanostructured palladium during potential cycling: a liquid-cell TEM study. Chemical Communications, 2019, 55, 9204-9207.	2.2	6
281	A nanoscale investigation on the influence of anodization parameters during plasma electrolytic oxidation of titanium by high-resolution electron energy loss spectroscopy. Applied Surface Science, 2021, 570, 151133.	3.1	6
282	Synthesis of high-oxidation Y-Ba-Cu-O phases in superoxygenated thin films. Physical Review Materials, 2018, 2, .	0.9	6
283	Electrolysis of glycerol to valueâ€added chemicals in alkaline media. Journal of Chemical Technology and Biotechnology, 2022, 97, 1950-1958.	1.6	6
284	Annealing Effects on the Chemical Configuration of Uncapped and (Poly-Si)-Capped HfO[sub x]N[sub y] Films Deposited on Si(001). Journal of the Electrochemical Society, 2005, 152, F101.	1.3	5
285	Correlative electron energy loss spectroscopy and cathodoluminescence spectroscopy on three-dimensional plasmonic split ring resonators. Microscopy (Oxford, England), 2018, 67, i40-i51.	0.7	5
286	Vertically Aligned Ni Nanowires as a Platform for Kinetically Limited Water-Splitting Electrocatalysis. Journal of Physical Chemistry C, 2019, 123, 1082-1093.	1.5	5
287	Microstructure and ferroic properties of epitaxial [γ-Fe2O3–BiFeO3]â^'Bi3.25La0.75Ti3O12 composite bilayers. Journal of Applied Physics, 2010, 108, 114111.	1.1	4
288	InAs quantum wire induced composition modulation in an In0.53Ga0.37Al0.10As barrier layer grown on an InP substrate. Journal of Applied Physics, 2010, 108, 034321.	1.1	4

#	Article	IF	CITATIONS
289	A "Thickness Series― Weak Signal Extraction of ELNES in EELS Spectra From Surfaces. Microscopy and Microanalysis, 2014, 20, 649-657.	0.2	4
290	Morphological evolution of Pt-modified nanoporous gold after thermal coarsening in reductive and oxidative environments. Npj Materials Degradation, 2020, 4, .	2.6	4
291	EELSpecNet: Deep Convolutional Neural Network Solution for Electron Energy Loss Spectroscopy Deconvolution. Microscopy and Microanalysis, 2021, 27, 1626-1627.	0.2	4
292	Analytical Electron Microscopy. Springer Handbooks, 2019, , 345-453.	0.3	4
293	Local Electronic Structure Of Defects In Gan From Spatially Resolved Electron Energy-Loss Spectroscopy. Materials Research Society Symposia Proceedings, 1997, 482, 784.	0.1	3
294	Probing the electronic structure of complex crystals with electron energy loss spectroscopy: a study ofnatisites. Journal of Physics Condensed Matter, 2006, 18, 3629-3637.	0.7	3
295	Effect of layer separation, InAs thickness, and rapid thermal annealing on the optical emission from a multi-layer quantum wire structure. Journal of Applied Physics, 2011, 109, .	1.1	3
296	Ultrastructural characterisation of the hydroxyapatite-coated pedicle screw and human bone interface. International Journal of Nano and Biomaterials, 2012, 4, 1.	0.1	3
297	Effects of Sample Preparation Technique on Quantitative Analysis of Automotive Fuel Cell Catalyst Layers. Microscopy and Microanalysis, 2014, 20, 472-473.	0.2	3
298	Reactions in a multilayered Si (substrate)/Ta/Mg/Fe/Ta/Pd thin-film structure during annealing and deuterium absorption. Acta Materialia, 2015, 90, 259-271.	3.8	3
299	Two-dimensional X-ray diffraction and transmission electron microscopy study on the effect of magnetron sputtering atmosphere on GaN/SiC interface and gallium nitride thin film crystal structure. Journal of Applied Physics, 2015, 117, 115301.	1.1	3
300	Core–Shell Nanocuboid Dimers with Nanometric Gaps. Journal of Physical Chemistry C, 2020, 124, 18690-18697.	1.5	3
301	Nanoscale Structural and Emission Properties within "Russian Dollâ€â€īype InGaN/AlGaN Quantum Wells. Advanced Optical Materials, 2020, 8, 2000481.	3.6	3
302	Materials Science Applications Of A Monochromated TEM. Microscopy and Microanalysis, 2003, 9, 112-113.	0.2	2
303	High-Resolution EELS and ab initio Study of the Oxygen K Edges in Bulk Perovskites. Microscopy and Microanalysis, 2004, 10, 852-853.	0.2	2
304	The Canadian Centre for Electron Microscopy: a national facility for ultrahigh resolution electron microscopy. International Journal of Nanotechnology, 2008, 5, 1082.	0.1	2
305	Structural investigation of interface and defects in epitaxial Bi3.25La0.75Ti3O12 film on SrRuO3/SrTiO3 (111) and (100). Journal of Applied Physics, 2013, 113, 044102.	1.1	2
306	A dominant electron trap in molecular beam epitaxial InAlN lattice-matched to GaN. Journal Physics D: Applied Physics, 2018, 51, 14LT01.	1.3	2

#	Article	IF	CITATIONS
307	The Performance of Electron Counting Direct Detection in Electron Energy Loss Spectroscopy. Microscopy and Microanalysis, 2019, 25, 586-587.	0.2	2
308	Eels Near Edge Structures. , 1999, , 265-300.		2
309	The effects of bending on plasmonic modes in nanowires and planar structures. Nanophotonics, 2022, 11, 305-314.	2.9	2
310	Electron Beam Induced Crystallisation in Iron (III) Fluoride. Materials Research Society Symposia Proceedings, 1995, 398, 195.	0.1	1
311	EELS Studies of B2-Type Transition Metal Aluminides: Experiment and Theory. Materials Research Society Symposia Proceedings, 1995, 408, 567.	0.1	1
312	Characterization of the Inhibition Layer on Galvanized Interstitial Free Steels. Microscopy and Microanalysis, 2002, 8, 358-359.	0.2	1
313	Machine-Learning Aided Evolution Studies of Nano-composite Electrodes and Nano-particle Catalysts for Fuel Cell Applications. Microscopy and Microanalysis, 2015, 21, 1063-1066.	0.2	1
314	Atomic Scale Structure and Chemistry Study of Franckeite - A Natural van-der-Waals Heterostructure - Using Scanning Transmission Electron Microscopy and Atom Probe Tomography. Microscopy and Microanalysis, 2020, 26, 1642-1643.	0.2	1
315	Selective area grown AllnGaN nanowire arrays with core–shell structures for photovoltaics on silicon. Nanoscale, 2021, 13, 8163-8173.	2.8	1
316	Platinum single-atom and cluster catalysis of the hydrogen evolution reaction. , 0, .		1
317	Atomic scale chemical ordering in franckeite—a natural van der Waals superlattice. Journal of Physics Condensed Matter, 2022, 34, 055403.	0.7	1
318	Electron ptychography dose reduction using Moiré sampling on periodic structures. Ultramicroscopy, 2022, 239, 113559.	0.8	1
319	Using EELS fine structures: understanding the chemical bond and obtaining spectroscopic images. Biology of the Cell, 1999, 91, 272-272.	0.7	Ο
320	The Effect of Local Symmetry on Atomic Resolution EELS Near-Edge Structures: Predictions for Grain Boundaries In NiAl. Microscopy and Microanalysis, 2000, 6, 186-187.	0.2	0
321	Characterization of Phase Transformation by Fe-SEM and Fe-TEM Analysis. Microscopy and Microanalysis, 2001, 7, 490-491.	0.2	Ο
322	Contributions of Microscopy to Advanced Industrial Materials and Processing. Microscopy and Microanalysis, 2002, 8, 188-189.	0.2	0
323	ELNES and EDS Mapping in HfOxNy Thin Films and AlN/TiN Superlattices. Microscopy and Microanalysis, 2004, 10, 308-309.	0.2	0
324	Transmission Electron Microscopy Studies of 5-cycled Na Alanate with Ti Based Additive. Materials Research Society Symposia Proceedings, 2005, 884, 1.	0.1	0

#	Article	IF	CITATIONS
325	Welcome from the Society Presidents. Microscopy and Microanalysis, 2006, 12, 54-54.	0.2	0
326	Advances in Electron Energy-Loss Spectroscopy with High Spatial and Energy Resolution. Microscopy and Microanalysis, 2014, 20, 2176-2177.	0.2	0
327	Response to: On the First Application of the Richardson–Lucy Algorithm to Resolve Plasmonic Resonances in EELS Spectra Obtained with a Monochromated Electron Beam. Microscopy and Microanalysis, 2014, 20, 995-995.	0.2	0
328	Aberration corrected STEM-EELS study of the hole distribution in cuprate superconductors. Microscopy and Microanalysis, 2015, 21, 665-666.	0.2	0
329	Surface Segregation of Fe in Pt-Fe Alloy Nanoparticles: Its Precedence and Effect on the Ordered-Phase Evolution during Thermal Annealing. ChemCatChem, 2015, 7, 3597-3597.	1.8	Ο
330	Thermally Driven Cation Exchange at Solid State between Cu2Se and CdSe Nanocrystals: an In-Situ TEM Study. Microscopy and Microanalysis, 2015, 21, 947-948.	0.2	0
331	In-situ Transmission Electron Microscopy to Probe the Electrochemical Deposition of Nanostructured Materials. Microscopy and Microanalysis, 2015, 21, 797-798.	0.2	0
332	Atomic Resolution Imaging and Spectroscopy of Pt-alloy Electrocatalytic Nanoparticles. Microscopy and Microanalysis, 2015, 21, 2247-2248.	0.2	0
333	Electrically injected AlGaN nanowire deep ultraviolet lasers. , 2016, , .		Ο
334	Advantages of Direct Detection and Electron Counting for High-Energy Resolution and Monochromated Electron Energy Loss Spectroscopy Data Acquisition. Microscopy and Microanalysis, 2018, 24, 474-475.	0.2	0
335	Understanding the Chemical and Relevant Phase Evolutions of Lithium-Based Electrode Materials Using Atomic-Resolution Electron Energy Loss Spectroscopy. Microscopy and Microanalysis, 2018, 24, 1520-1521.	0.2	0
336	Atomic-resolution Imaging and Spectroscopy of Iron Oxide Epitaxial Thin Films. Microscopy and Microanalysis, 2018, 24, 1614-1615.	0.2	0
337	Surface Plasmon Resonance Mode Behaviour in Sierpinski Fractal Triangles and New Plasmonic Materials. Microscopy and Microanalysis, 2019, 25, 636-637.	0.2	0
338	Large Field of View Strain Characterization in a Scanning Transmission Electron Microscope Using a Designed Coherent Sampler. Microscopy and Microanalysis, 2019, 25, 86-87.	0.2	0
339	The in situ Studies on the Anomalous Domain Switching Caused by Trace Amount of Oxygen Vacancies. Microscopy and Microanalysis, 2019, 25, 1888-1889.	0.2	0
340	Rücktitelbild: Ternary Snâ€Tiâ€O Electrocatalyst Boosts the Stability and Energy Efficiency of CO ₂ Reduction (Angew. Chem. 31/2020). Angewandte Chemie, 2020, 132, 13224-13224.	1.6	0
341	Surface Plasmonic Properties of Wrinkled Gold Wires and Films : An electron energy loss spectroscopy & microscopic polarization modulation infrared study. , 2020, , .		0
342	Strong Phonon-Plasmon Coupling Between Nanoscale Antennas. Microscopy and Microanalysis, 2020, 26, 1498-1500.	0.2	0

#	Article	IF	CITATIONS
343	Comparison Between Moiré Sampling Scanning Transmission Electron Microscopy Geometrical Phase Analysis Strain Characterization Method and Dark-Field Electron Holography. Microscopy and Microanalysis, 2021, 27, 1982-1984.	0.2	Ο
344	Crystal Lattices Reconstruction from Moiré Aliased Scanning Transmission Electron Microscopy Electron Microscopy and Microanalysis, 2021, 27, 1986-1988.	0.2	0
345	Near-Infrared Cathodoluminescence Polarimetry of a Plasmonic Vertical Split Ring Resonator. Microscopy and Microanalysis, 2021, 27, 706-708.	0.2	Ο
346	Crystal lattice image reconstruction from Moiré sampling scanning transmission electron microscopy. Ultramicroscopy, 2022, 233, 113426.	0.8	0
347	Wrinkled Film Optics: From Infrared Electromagnetic Hotspots to Plasmon- Enhanced Electrochemistry. , 2021, , .		0